Combination of Finite Element and Analytical Models in the Optimal Multi-Domain Design of Machines : Application to an Interior Permanent Magnet Starter Generator

Jérome Legranger *[x], Guy Friedrich[x], Stéphane Vivier[x], and Jean Claude Mipo*
* Valeo Electrical System
2, Rue André Boulle / BP150
94017 Créteil Cedex / France
Email: jerome.legranger@utc.fr and jean-claude.mipo@valeo.com
[x] Université de Technologie de Compiègne
EA 1006 Laboratoire Electromécanique de Compiègne/ BP20529
60205 Compiègne Cedex / France
Email: guy.friedrich@utc.fr and stephane.viver@utc.fr

***Abstract*— This paper proposes to apply optimal multiphysic models to the design of highly constrained electrical machines, such as interior permanent magnet machine (IPM) intended for an automotive integrated starter generators (ISG). One of the main problems in the use of such optimal approaches remains the accuracy of the models used by the optimizer. In a previous paper [1], we proposed a design model linked to three strong hypotheses : 1) Iron losses are calculated according to the flux density fundamental (sinusoidal approach) 2) Flux densities are estimated with a saturated but decoupled d,q reluctant circuit model neglecting the cross saturation effect 3) Thermal states are indirectly treated with a current density limit. The present paper improves theses models by using first the finite element method (FEM) for the determination of flux and iron losses in the machine and then an equivalent thermal steady state lumped parameter network. These models are included in the optimization loop and so are evaluated at each iteration. The optimization method uses standard sequential quadratic programming algorithm (SQP) and Sequential Simplex algorithm. A comparison between the design of an IPM machine with the previous model and the new one will be performed.**

I. Introduction

Interior permanent magnet synchronous machines are attractive candidates for automotive applications such as the Toyota Prius motor or integrated starter generator (ISG) [3] because of their high efficiency (low-loss rotor), a brushless design, a high torque/power density and a wide constant-power speed range [2], [4]–[7].

However, optimal design of ISG IPM applications is subject to very constrained and even contrary requirements [8]. First, a high starting torque in a limited core volume (for cost reduction) induces a high saturation level in the machine. Then, a low back-EMF at high speed is required to partly avoid the risk of high voltage in the case of a default of the power converter. Finally, electromechanical torque and high generating power specifications must be met according to thermal constraints since the under-the-hood temperatures can rise above 120°C.

As a result, optimization techniques have proved to be compulsory to obtain optimal drives. They require different type of choices, such as the following :

- optimization variables, objective function and constraints
- algorithm of optimization
- accurate, flexible and fast multi-domain models of the machine

The choice of the optimization variables are bound to the specification book whereas the selection of optimization algorithms is generally related to the designer's experience [1]. Publications propose either the use of rules of art for determining some design variables [8] along with a deterministic algorithm (sequential quadratic programming...) or specific stochastic algorithms (Monte Carlo [9], genetic..) [10]. Nevertheless, the use of a fast and accurate enough model of the machine suffers no compromise.

The purpose of this paper is to present an improved multi-domain model of the IPM ISG developed in [1] to be integrated in an optimizer. In fact, a map of the flux density in the machine including cross-saturation effects is obtained with a 2D finite element models and dq frame theory. Iron losses are determined according to Bertotti formula and the shape of the flux density in the machine core without first harmonic hypothesis. Finally, a three-dimensional thermal lumped-parameter network instead of a current density limit estimates the true machine temperatures at key points such as the windings. The models are linked and implemented in a Sequential Simplex optimization algorithm. The magnetic model is validated by experimental results whereas the thermal model presents good agreement with detailed thermal finite element method.

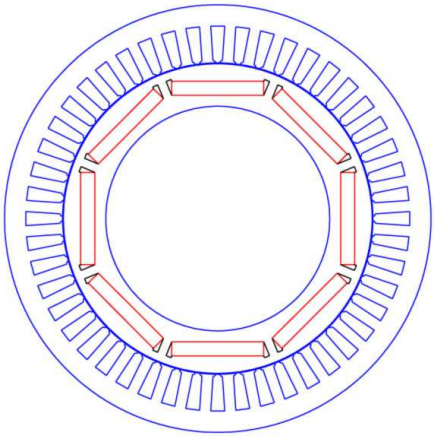

Fig. 1. The studied cross section of the ISG

II. Machine optimal design approach

The optimal design tool is based on a Sequential Simplex optimizer to minimize the IPM machine length (figure 1) according to torque (cranking torque, high speed torque), power (several generating power points) and efficiency requirements of ISG applications.

More specifically, the algorithm uses the same discrete and continuous optimization variables and constraints presented in [1], that is to say :

- rotor variables : l_a (magnet height), w_1, h_{cr}, t_{cr} (iron gap data)
- stator variables : ent (airgap length), R_{is} (airgap diameter), ratiobzsbes (teeth/slot width ratio), h_{esbob} (slot height)
- other variables : L_{zs} (stack length), N_s (turn number)

The initial solution of the optimization is found by applying rules of art like the D^2L method or [8].

The multi-domain model combines a finite element magnetic model of the IPM machine that aims at determining a map of the machine flux linkages with a 3D thermal resistance network and an optimal electric model based on dq frame and loss minimization approach (figure 2). The link between the model relies on two internal loops :

- temperatures modifying both the copper resistivity and thermal characteristic of air
- currents determining the magnetic saturation state along with iron and copper losses

Both flux linkage map and temperature estimation are fully automated and integrated in the Simplex optimizer.

III. Electromagnetic finite element Model

The magnetic model is based on the dq transformation with the only assumption that the magnetization curves are independent of the rotor position θ [11]. The flux linkages Ψ have so the following form :

$$\Psi_d(i_d, i_q, \Psi_{ap}) \; and \; \Psi_q(i_d, i_q) \tag{1}$$

where i_d and i_q are the d and q axis currents. As a result, both the cross coupling and saturation effect are taken into account.

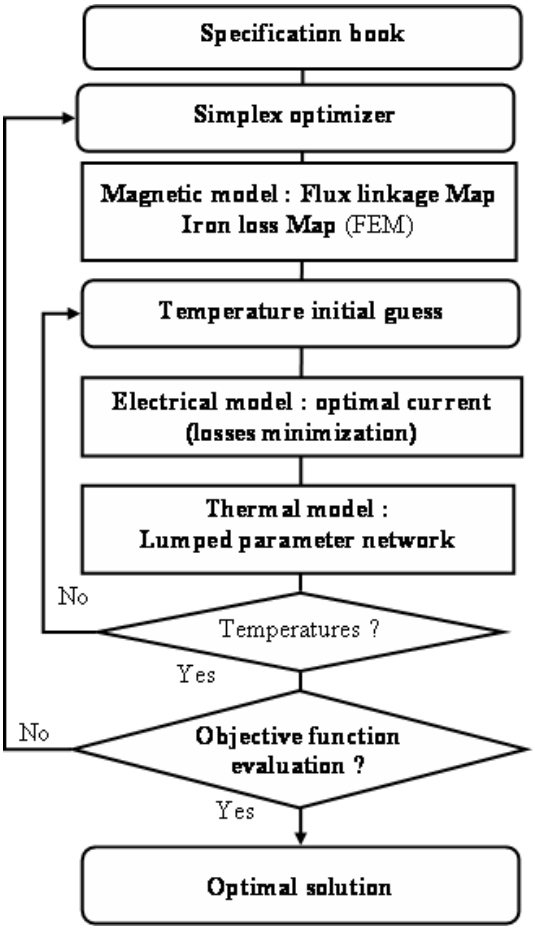

Fig. 2. Flowchart of the optimization method

The calculation of the d and q flux linkages map is automatically performed at each step of the optimization process with 2D magnetostatic FEM (MATLAB Pdetool or other FEM tool) as in [11] by first setting the magnet remanence B_r to the required value. Then appropriate currents are injected in both d and q axis (cross coupling effect) according to the winding distribution. Finally, the flux linkages are calculated in the three phases (a,b,c) of the machine and converted to dq frame by a reverse Park Transformation.

The end leakage inductance is calculated separately using empirical formula of [12].

The q flux linkage mapping (figure 3) of the IPM machine presented in [1] demonstrates a high cross coupling between Ψ_q and i_d.

The number of calculation points of the flux map is carefully chosen to reduce computation time since the model is fully integrated in an optimization loop.

One of the major objective of this transformation is to accurately predict the electromagnetic torque T_e produced by the machine which is given by :

$$T_e = \frac{3}{2} p \left(\Psi_d i_q - \Psi_q i_d \right) \tag{2}$$

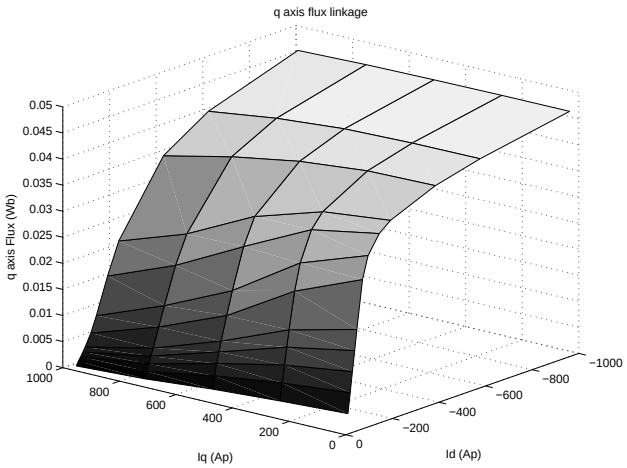

Fig. 3. q axis flux linkage including cross saturation effect

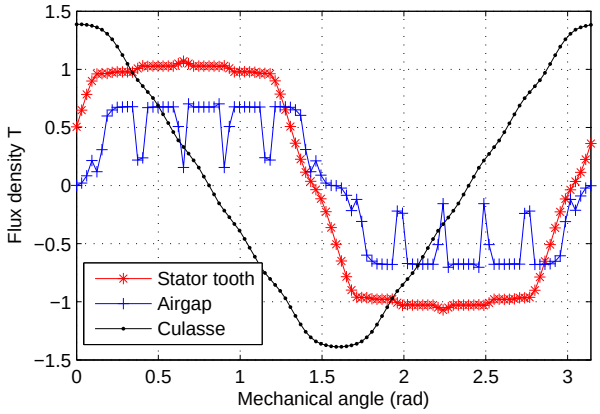

Fig. 4. No load flux density in stator and airgap of the IPM

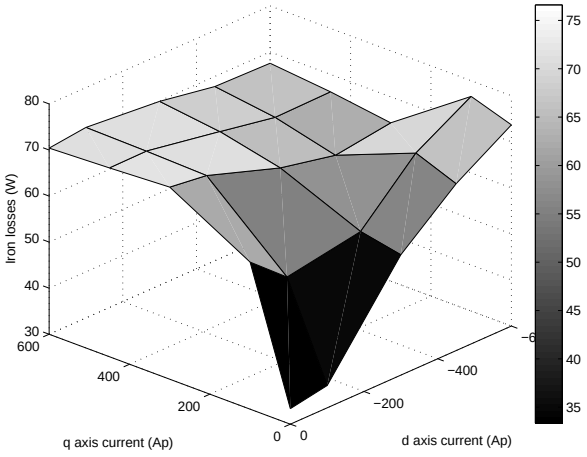

Fig. 5. Map of iron losses at 1000 rpm

IV. Iron losses model

Different methods allow the prediction of iron losses such as empirical formula (Steinmetz, Bertotti) or finite element prediction methods (Preisach or Jiles Atherton...). They differ from the:

- choice of flux density shape : simple assumption of linear trapezoidal variation of time based finite element variation
- accuracy : first harmonic hypothesis, rotational field losses prediction, hysteresis minor cycle estimation
- computation time

As our model is a design model for ISG, rotor losses due to airgap flux harmonics, are accounted for with formula of [13] assuming that the losses are located near the airgap and mainly due to the slotting effect.

For the stator, a trade off consists in determining the tooth and core flux density waveform from the radial flux density in the airgap calculated in the magnetic model using a simple flux conservation law neglecting the flux leakage (figure 4). For the tooth, the formula yields :

$$B_t(\theta) = \frac{1}{b_{zs}} \int_{\theta}^{\theta+\tau_s} B_{ent}\ R_{is}\ d\alpha \tag{3}$$

where b_{zs} is the tooth width, τ_s the tooth span, R_{is} the airgap radius and B_{ent} the radial flus density in the airgap.

Then, a map of iron losses is determined using Bertotti formula (figure 5) that separates the losses into :

- Hysteresis losses
- Eddy current losses

Iron loss are 2 times lower at no load than at full load due to the high harmonic content of the flux density rather than its fundamental which mainly occurs during flux weakening operations. It consists of the major improvement of the method compared with no load irons losses estimation.

V. Electrical model

The electrical model consists of a SQP optimizer that determines for each torque-speed characteristics the optimum current to minimize the total losses and deliver the required torque or power at the required speed without exceeding the battery voltage and power limits. It relies on both the d-q model assumption and the hypothesis that the voltage and currents waveform are sinusoidal.

So, the machine voltage equations are reduced to :

$$v_d = Ri_d - \omega_e\ \psi_q(i_d, i_q) \tag{4}$$
$$v_q = Ri_q + \omega_e\ \psi_d(i_d, i_q) \tag{5}$$

and the maximum value of the machine peak voltage is limited to half the battery voltage ($U_{dc}/2$).

VI. Thermal model

For an optimal design stage, 3D lumped parameters thermal models (figure 6) provide a fast mean of estimating temperatures inside the machine at the cost of accuracy compared to FEM results. The model has been developed to study transient and steady state thermal analysis and relies on the IPM decomposition in elementary thermal convection or conduction cells.

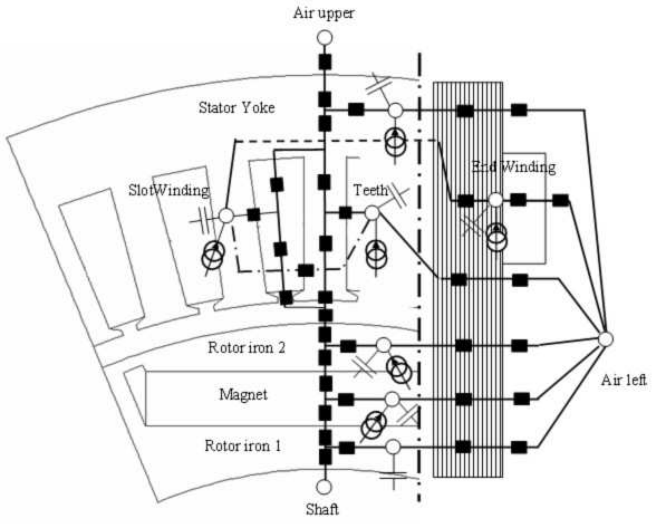

Fig. 6. Lumped parameters thermal network

The model is implemented with the following assumptions :

- the shaft temperature and ambient temperature are specification book data
- the ISG is air cooled with axial fins

A. Conduction cells

Conduction cells allow the determination of the average temperature of each solid part thanks to the resolution of the heat transfer equation assuming that heat sources are uniformly distributed in the volume, heat flux is unidirectional and material is uniform.

The determination of the winding equivalent thermal conductivity encompasses the filling factor effect, the average disposition of the winding in the slot and the number of conductor per slot [14] whereas thermal conductivity of iron is simply anisotropic.

Thermal capacities are calculated according to the average mass and average specific heat capacity of the material.

B. Convection cells

Convection coefficients depend on the nature of the convection (natural, mixed or forced), the nature of the air flow (laminar or turbulent) and the air temperature. These coefficients are obtained by empirical correlations [15] mainly based on two adimensionnal numbers :

Nusselt number Nu that describes the relationship between convective heat transfer and conductive heat transfer :

$$h = Nu\,\frac{\lambda_{air}}{D_h} \tag{6}$$

where h is the convection heat transfer coefficient, λ_{air} is the thermal conductivity of the fluid and D_h is the hydraulic diameter.

Reynolds number that characterizes the air flow :

$$Re = \frac{\rho\, v_{av}\, D_h}{\eta} \tag{7}$$

In this expression v_{av}, η and ρ represent respectively the radial flow velocity, dynamic viscosity and density of air.

1) Rotor ends : Rotor ends are assumed to be smooth discoid rotating surfaces subjected to forced convection. Among all the authors that deal with this geometry [14], we choose Dorfman and Kreith correlation, which states that the convection coefficient for laminar flow with a Reynolds number below 250000 is :

$$h_c = 0.35\ \lambda_{air}\ \left(\frac{\omega}{\upsilon}\right)^{1/2} \tag{8}$$

For turbulent flow, with a Reynolds number above 250000 :

$$h_c = 0.0195\ \frac{\lambda_{air}}{R_{er}}\ \left(\frac{\omega\ R_{er}^2}{\upsilon}\right)^{0.8} \tag{9}$$

where R_{er} is the rotor external radius, ω the rotor speed , and υ the cinematic viscosity of air.

2) Airgap: Convection heat transfer coefficient in the airgap are considered according to Taylor's formula [15]- [16]. In the analytical calculation, the Taylor number (Ta) is used to judge if the flow is laminar, vortex or turbulent :

$$Ta = \frac{\omega^2\ R_{airgap}\ g^3}{\upsilon^2} \tag{10}$$

where g is the airgap height, R_{airgap} is the airgap radius and ω the rotor speed.

If $Ta < 1700$, the flow is laminar and Nu=2.

If $1700 < Ta < 10^4$, the flow takes on vortex and $Nu = 0.128\ Ta^{0.367}$.

If $10^4 < Ta < 10^8$, the flow become fully turbulent increasing the Nusselt number : $Nu = 0.409\ Ta^{0.241}$.

3) Stator outer surface: The convection coefficient of the stator outer surface is calculated in two steps. First, the surface is assumed to be smooth (no fins). Therefore the convection coefficient is estimated with Churchill and Chu correlation of free convection on a horizontal cylinder :

$$Nu = \left(0.6 + 0.387\left(\frac{Ra_D}{\left(1+\left(\frac{0.559}{Pr}\right)^{9/16}\right)^{16/9}}\right)^{1/6}\right)^2 \tag{11}$$

with the Rayleigh number :

$$Ra_D = \frac{g\ \beta\ Pr}{\upsilon^2}\ D_h^3\ (T_{stator} - Tair) \tag{12}$$

where g is the gravitational force of attraction, T_{air} and T_{stator} are the temperature of the air and the stator, β the fluid coefficient of cubical expansion and Pr the Prandtl number. These two latter are evaluated at the temperature $((T_{air} + T_{stator})/2)$.

Then, heat transfer coefficients calculated with smooth surface are increased with m :

$$m = \xi\ \frac{S_{smooth}}{S_{fin}} \tag{13}$$

where S_{smooth} is the area without fins, S_{fins} is the total area with fins. The fin efficiency ξ is given by the formula :

$$\xi = \frac{1}{nd}\ \frac{\frac{h}{nd} + tanh\,(nd)}{1 + \frac{h}{nd}\,tanh\,(nd)}\ and\ n = \sqrt{\frac{2\,h}{\lambda\,L}} \tag{14}$$

where d is the fin length, L the fin width, h the heat transfer coefficient and λ the fins thermal conductivity.

C. Radiation cells

Assuming that the outer surface of the stator is a diffusive gray body, the radiation heat transfer coefficient h_r is calculated with Stefan Boltzman law :

$$h_r = \epsilon_r \, \sigma \, (T_{surface} + T_{air}) \, (T_{surface}^2 + T_{air}^2) \qquad (15)$$

with σ the Bolztmann constant.

VII. Machine performance comparison

After implementing the optimized machine models described in section II and III, the IPM machine optimal design software was exercised to provide a comparison with the method developed in [1]. The key differences between the methods (table I) consists of the winding temperature estimation along with a more accurate iron and mechanical losses computation. In order to develop a comparison between the methods, the same specification book, objective function and constraints are assigned to the optimizers.

Models	Baseline : method [1]	Presented method
Electromagnetic	Analytical Decoupled	Finite elements Cross saturation
Losses	No-load iron losses	Load iron losses
Thermal	Current densities	Winding temperatures
Electrical	Minimal copper losses	Optimal efficiency

TABLE I

Comparison of the two optimal methods

A. Specification book

In ISG application, the objective is to reduce the length of the electric machine to be integrated next to the thermal engine without modification of the vehicle.

The constraint function is of four types.

First, torque-speed characteristic :

- Starter mode : 140 N.m from 0 to 100 rpm
- Generator mode (G1) : 4900 W at 2000 rpm with minimum efficiency of 0.8
- Generator mode (G2) : 3400 W at 5000 rpm

For geometric constraints, the external diameter is set to 255 mm and the internal diameter is set to 134 mm.

For supply constraints, the ISG is supplied by a 42 Vdc battery with a 20 $m\Omega$ internal resistance and a 10 kW maximum power.

The thermal constraints consist of a maximum temperature of 180°C for the windings. The air temperature is set to 20°C, and the shaft temperature to 40°C according to the specification book of [1].

Finally, the same iron sheet material (M45) and permanent magnets have been implemented.

B. Optimized Machines

Table II provides a summary of the key dimensions and parameters of the optimized IPM machines for a starter/alternator application with the models of [1] (Design 1) and the presented models (Design 2). Figures 7 and 8 provides cross sectional views of one pole of both machines.

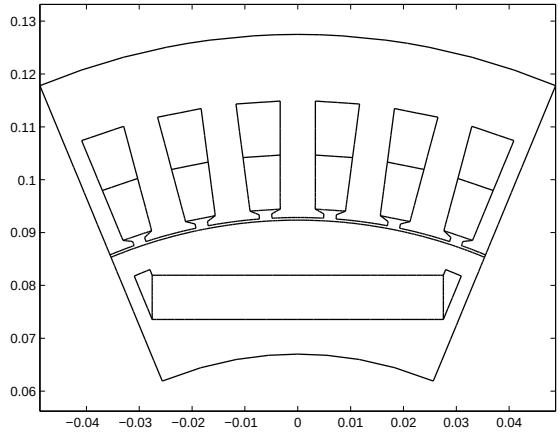

Fig. 7. Cross section of one pole of the Design 1 with models of [1]

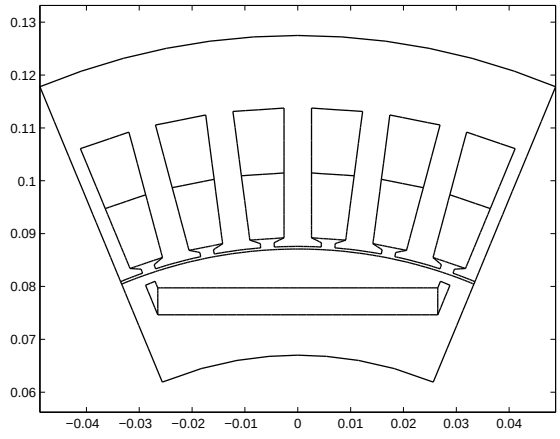

Fig. 8. Cross section of one pole of the Design 2

As indicated the design using the new multi-physic model achieves its primary goal of reducing the total length and weight of the machine with respectively a length of 66.2 mm and 80.7 mm. Nevertheless, that result requires a few observations.

The starter point and especially the battery power limit (10 kW) conditions by far the design 2. The windings temperatures in starter or generator mode (G1 and G2) are 20°C lower than the maximum allowable temperature of 180°C whereas the required efficiency in G1 point is ten percentage point higher than the 0.8 efficiency constraint.

For the starter point, the temperature guess of the design 1 and the calculated temperature of design 2 are quite similar. In fact, the starting time of an ISG is generally far less than one minute and the high thermal capacities of the machine prevent windings temperatures to rise sharply despite the amount of copper losses (8.5 kW and efficiency of 14 %). Nevertheless, the thermal model constraint of design 2 does not limit the

	Design 1	Design 2
Number of Poles	8	8
Iron material	M45	M45
Slot number	48	48
Turn number	24	24
Magnet remanent	1.1 T	1.1 T
Rotor Inner radius	67 mm	67 mm
Stator outer radius	127.5 mm	127.5 mm
Airgap radius	92.8 mm	87.6 mm
Thickness of magnet	8.4 mm	5.2 mm
Slot height	20.4 mm	24.4 mm
Bridge thickness	4.8 mm	1.7 mm
Active length	32.0 mm	18.7 mm
Total length	80.9 mm	66.2 mm
Total weight	10.6 kg	8.0 kg
Starter Temperature	30°C	35°C
Starter Current	510 Aeff	842 Aeff
Starter Efficiency	0.23	0.14
Starter Required Power	7.5 kW	10 kW
G1 Temperature	180°C	159°C
G1 Current	117 Aeff	135 Aeff
G1 Efficiency	0.88	0.90
G2 Temperature	180°C	156°C
G2 Current	137 Aeff	112 Aeff
G2 Efficiency	0.65	0.75

TABLE II

COMPARISON OF MACHINES PARAMETERS FOR THE TWO DESIGNS

optimizer whereas the current density contraint (25 A/mm^2) of design 1 is the limiting point of the sizing.

For the first generating point, despite the required RMS current in design 2 is higher than in design 1, the efficiency of the machine is roughly the same. The underlying reason of this constatation is first that windings temperature of design 1 is 20°C higher than design 2 and that electrical model of design 2 looks for the current both in magnitude and phase to minimize the total losses and not only copper losses as in design 1.

For the generating point 2, the efficiency of design 2 is even better than design 1. In fact, due to the low DC voltage of 42 Vdc the IPM machine is subject to a high demagnetizing current at 5000 tr/min (d axis current of -158 Ap and q axis current of -19 Ap) to compensate the high electromotive force. As a result, flux estimation are sensitive to cross coupling effect and therefore to the optimal current calculation of the electrical model.

Finally, the dimensions of the iron bridges are reduced from 4.8 mm to 1.7 mm. An explanation for this difference can be found in the fact that iron bridges height of design 2 are calculated using analytical mechanical stress method (centrifugal forces stress on bridge compared to yield stress of M45 material) whereas for design 1 the minimal height is set to 4.5 mm. As a result, the required flux to saturate the bridge is lower for the design 2 and the magnets height is reduced accordingly.

VIII. CONCLUSION

A coupled multi-domain model linked with a Sequential Simplex optimizer for IPM has been presented. Models are a trade off between required accuracy and computation time. The magnetic model combines a dq transformation along with FEM flux linkage calculation to estimate the d and q flux linkage in the IPM enabling an accurate calculation of the torque with cross saturation effect.

Iron loss model consists of an estimation of the flux density waveform in the stator thanks to the flux conservation rule and the flux density mapping of the magnetic FEM model along with Bertotti empirical formula. The harmonic content of flux density during flux weakening operations is so properly taken into account.

The thermal model is a 3D transient lumped parameters network to predict the temperatures of key points inside the machine including stator windings and rotor magnets.

In our example, the proposed method allows to reduce the total weight of 20 % and the magnets weight of 60 %. The thermal model shows the high influence of the external parameters on the machine design.

The model is versatile enough to compute any kind of magnet shape including double layer magnets.

REFERENCES

[1] L. Chédot, G. Friedrich and J.M. Biedinger, *Integrated Starter Generator : The need for an Optimal Design and Control Approach. Application to a Permanent Magnet Machine*, IEEE Trans. on Ind. Appl., vol. 43, No.2,pp. 551-559, Mar./Apr. 2007.

[2] R.F. Schiferl and T.A. Lipo, *Power capability of salient pole permanent magnet synchronous motors in variable speed drive applications*, IEEE Trans. on Indus. Appl., vol. 26, no. 1, pp. 115-123, Jan./Feb. 1990.

[3] E. C. Lovelace, T. M. Jahns, J. L. Kirtley Jr. and J. H. Lang, *An interior PM starter/alternator for automotive applications*, Proc. Int. Conf. Elect. Mach., vol. 3, pp. 1802-08, 1998.

[4] B. Chalmers, L. Musaba and D. Gosden, *Variable-frequency synchronous motor drives for electrical vehicles*, IEEE Trans. Ind. Appl., vol. 32,no. 4, pp. 896-903, Jul./Aug. 1996.

[5] J. Hadji-Minaglou and G. Henneberger, *Comparison of different motor types for electric vehicle application* ,EPE J., vol. 8, no. 3/4, pp. 46-55, Sep. 1999.

[6] G. Friedrich, L. Chédot and J.M. Biedinger, *Comparison of two optimal machine design for integrated starter-generator applications*, in Proc. Int. Conf. Elect. Mach., Aug. 2002, CD-ROM.

[7] R. Dutta and M.F.Rahman, *A segmented magnet interior permanent magnet machine with wide constant power range for application in hybrid vehicles*,Vehicle Power and Propulsion Conf., 2005.

[8] B-H. Bae and S.K. Sul, *Practical design criteria of interior permanent magnet synchronous motor for 42V integrated starter-generator*, IEMD03 Conf., vol. 2, pp. 656-662, 2003

[9] A.M. EL-Refaie, N.C. Harris, T.M. Jahns and K. M. Rahman, *Thermal analysis of multibarrier interior PM synchronous Machine using lumped parameter model*, IEEE Trans. on . Ener. Conv., vol. 19, No. 2, pp. 303-309, June 2004.

[10] I. Klumpner, D. Risticevic, and I. Boldea, *Advanced optimization design technique for automotive permanent magnet synchronous machine* , Proc. Int. Conf. Elect. Mach. and Drives, pp. 227-234, May 2005.

[11] T.J.E. Miller, M. Popescu, C. Cossar and M. McGilp, *Performance estimation of interior permanent-magnet brushless motors using the voltage-driven flux-MMF diagram*, IEEE Trans. on Magnetics, vol. 42, no. 7, pp. 1867-1872, Jul. 2006.

[12] M. Liwschitz, *Calcul des machines électriques*, Book SPES Lausanne, 1969.

[13] L. Albert, *Modélisation et optimisation des alternateurs à griffe, application au domaine automobile*, PhD Thesis INPG, 2004.

[14] B. Renard, *Etude experimentale et modélisation thermique du comportement d'une machine électrique multi-fonction*, thesis, ENSMA, Poitiers, 2003

[15] F.P Incropera, D.P. Dewitt, *Introduction to heat transfer, Third Edition*, (John Wiley and Sons, 1996)

[16] G. I. Taylor, *Distribution of velocity and temperature between concentric cylinders*,Proc. Roy. Soc., 546-578, (1935)